High Voltage Driven MnO_2/CuO for Efficient Oxidation of 5-Hydroxymethylfurfural

Mengyang Yin [a], *Hongliang Dai* [a], *Xi Chen* [a], *Weiqiang Fan* [a,c]*, *Hongye Bai* [a,b]*

[a] *School of Chemistry and Chemical Engineering, Jiangsu University, Zhenjiang, 212013, PR China.*

[b] *Key Laboratory of Advanced Energy Materials Chemistry (Ministry of Education), Nankai University, Tianjin 300071, China*

[c] *Key Laboratory of Green Extraction and Efficient Utilization of Light Rare-Earth Resources (Ministry of Education), Baotou, 014010, China.*

E-mail: bhy198412@163.com, fwq4993329@ujs.edu.cn.

Experimental

Chemicals

All chemicals and reagents are purchased from Shanghai Macklin Biochemical Technology Co., Ltd.

Synthesis of MnO_2

0.51 g $Mn(NO_3)_2 \cdot 4H_2O$ and 1.30 g dimethylimidazole are added to 40 mL deionized water, respectively. The two solutions are mixed and stirred at room temperature for 10 min. Ni foam (1×2 cm^2) is vertically immersed into the above solution for 0.5 h to obtain Mn_3O_4. Finally, the MnO_2 are obtained after activation by cyclic voltammetry (CV).

Synthesis of CuO and MnO_2/CuO

In a three-electrode system (Ag/AgCl as the reference electrode, Pt wire as the counter electrode, Ni foam or MnO_2 as the working electrode), precursor is prepared by deposition at a constant voltage (-1.2 V vs Ag/AgCl) for 200 s using 0.05 mol/L $Cu(NO_3)_2$ as the electrolyte. The samples are activated by CV operation in 1.0 M KOH (-0.7 to 1.8 V_{RHE}), CuO and MnO_2/CuO are then obtained.

Physical characterization

In this experiment, the crystal structure of samples is determined by X-ray diffractometer (XRD, SmartLab). Surface morphology and phases of samples are investigated by scanning electron microscopy (SEM, Apreo S HiVac) and high resolution transmission electron microscopy (HRTEM, JEM-2100). The chemical bonding is studied by Raman spectroscopy (Raman, DXR). The chemical composition is determined by X-ray photoelectron spectroscopy (XPS, ESCALAB QXi).

Electrochemical experiments

All electrochemical performances are studied on CHI 1440D electrochemical

workstation. Electrochemical experiments are carried out in a three-electrode system, with Hg/HgO electrode as the reference electrode, Pt wire as the counter electrode, samples as the working electrode and 1.0 M KOH as the electrolyte.

Quantitative analysis of products

20 uL reaction solution is taken out and then diluted to 2 mL. The diluted reaction solution is detected by high performance liquid chromatography (HPLC). Mobile phase A is 5 mM ammonium formate solution, and mobile phase B is 10% methanol solution. The ratio of mobile phase A to B is 8:2 (flow rate 0.6 mL/min, elution time 14 min). Finally, the reactants and products are quantitatively analyzed by the external standard method. HMF conversion, FDCA yield and Faraday efficiency (FE) are calculated according to the following equations:

$$\text{HMF conversion (\%)} = \frac{\text{mole of consumed HMF}}{\text{mole of initial HMF}} \times 100\%$$

$$\text{FDCA yield (\%)} = \frac{\text{mole of FDCA formed}}{\text{mole of initial HMF}} \times 100\%$$

$$\text{FE of FDCA (\%)} = \frac{\text{mole of FDCA formed}}{\text{total charge passed}/(6\times F)} \times 100\%$$

Measurement in continuous flow electrolytic cell

Compared with H-type electrolytic cell, the continuous flow electrolytic cell can realize the continuous supply of reactants and product of FDCA, which effectively prevents the polarization of solution concentration and improves the mass transfer efficiency of substances. Two separate electrolytic cells are connected using peristaltic pumps. The MnO_2/CuO with an area of 1 cm^2 are prepared and mounted on the anode of the continuous flow electrolytic cell, and proton exchange membrane is installed between the anode and the cathode.

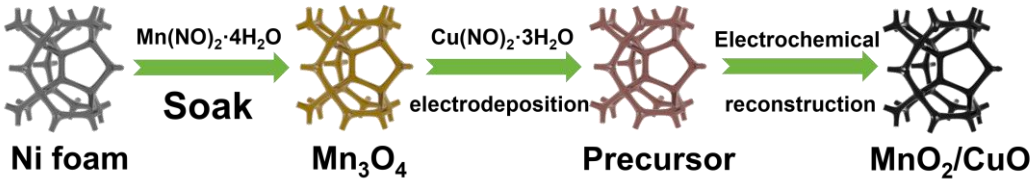

Fig. S1. Schematic diagram of the synthesis process of MnO_2/CuO.

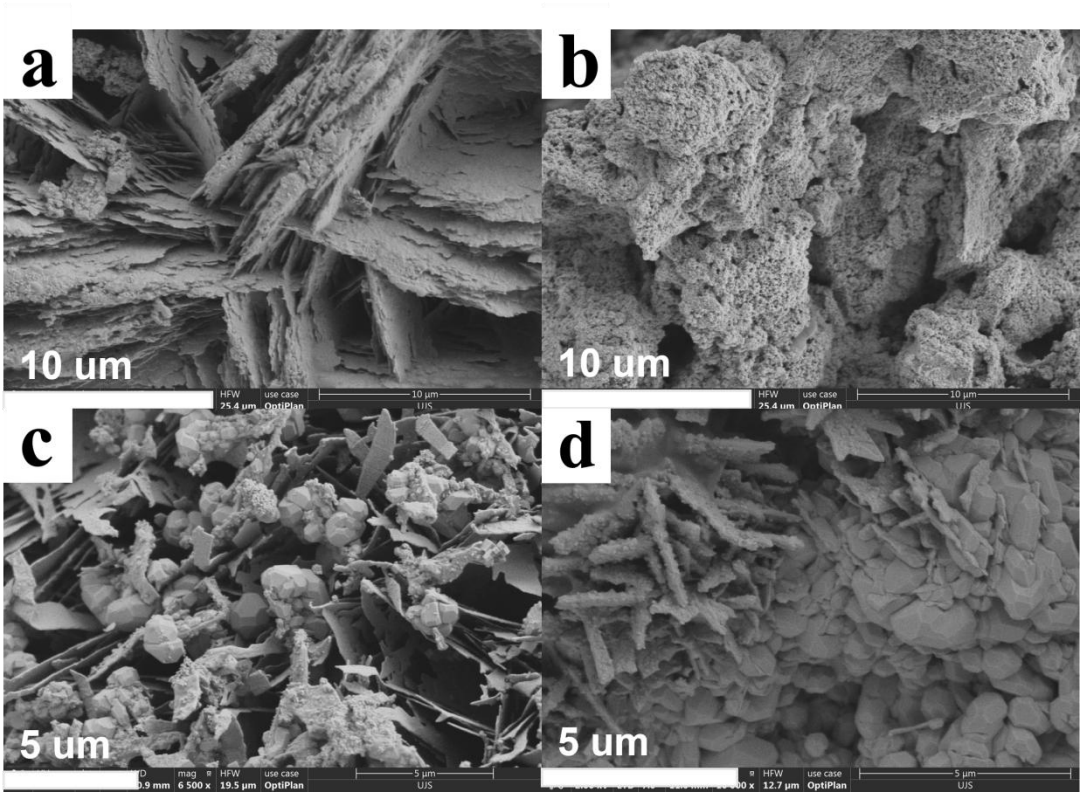

Fig. S2. SEM images of (a) Cu_2O, (b) Mn_3O_4, (c) Precursor, and (d) MnO_2/CuO (low magnification).

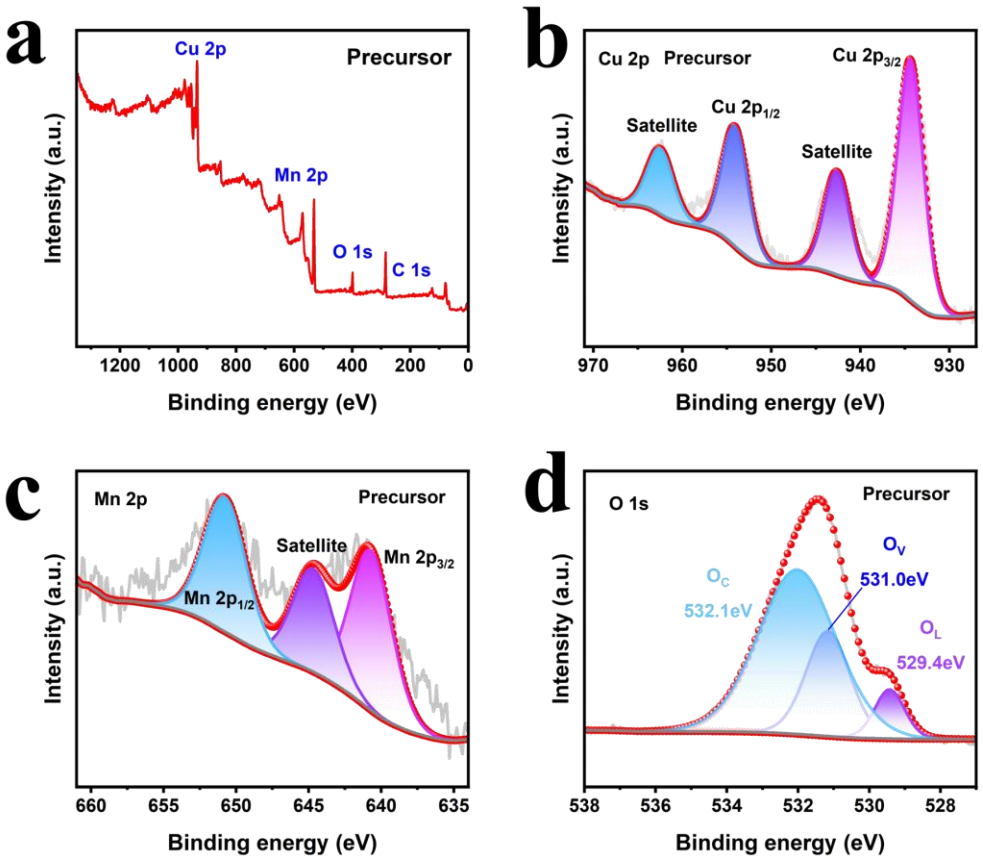

Fig. S3. (a) Full-scan XPS spectra of precursor. XPS survey spectra of (b) Cu 2p, (c) Mn 2p, and (d) O 1s.

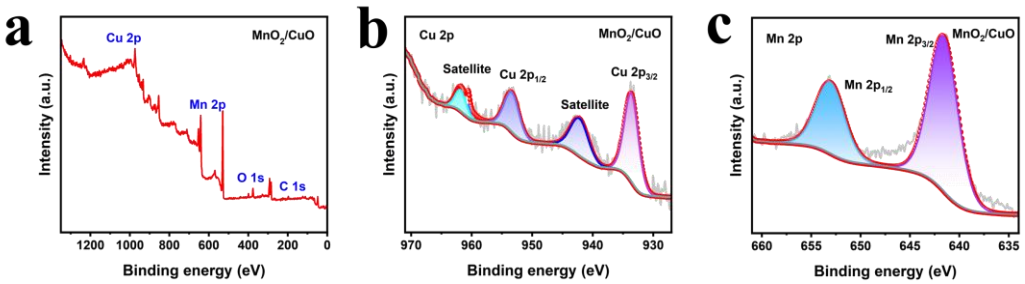

Fig. S4. (a) Full-scan XPS spectra of MnO_2/CuO. XPS survey spectra of (b) Cu 2p, and (c) Mn 2p.

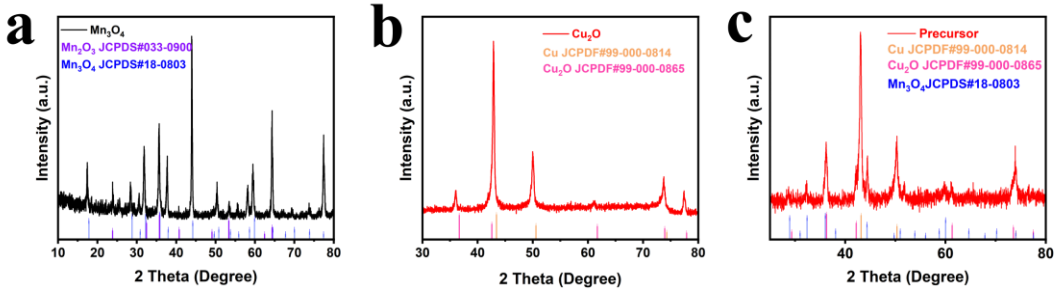

Fig. S5. XRD patterns of (a) Mn_3O_4, (b) Cu_2O, and (c) Precursor.

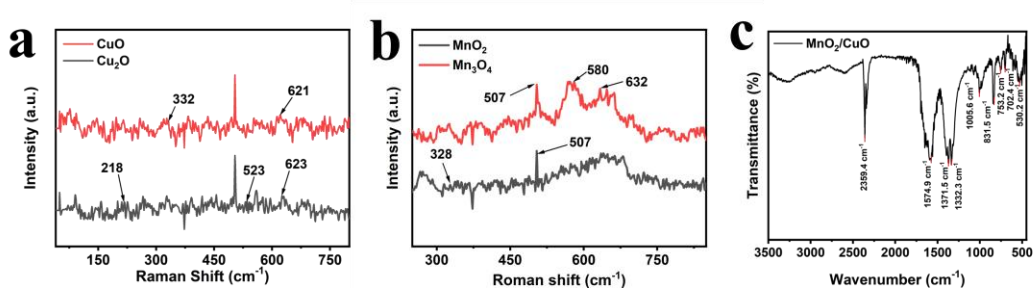

Fig. S6. Raman spectra of (a) CuO, and (b) MnO_2. (c) FT-IR spectrum of MnO_2/CuO.

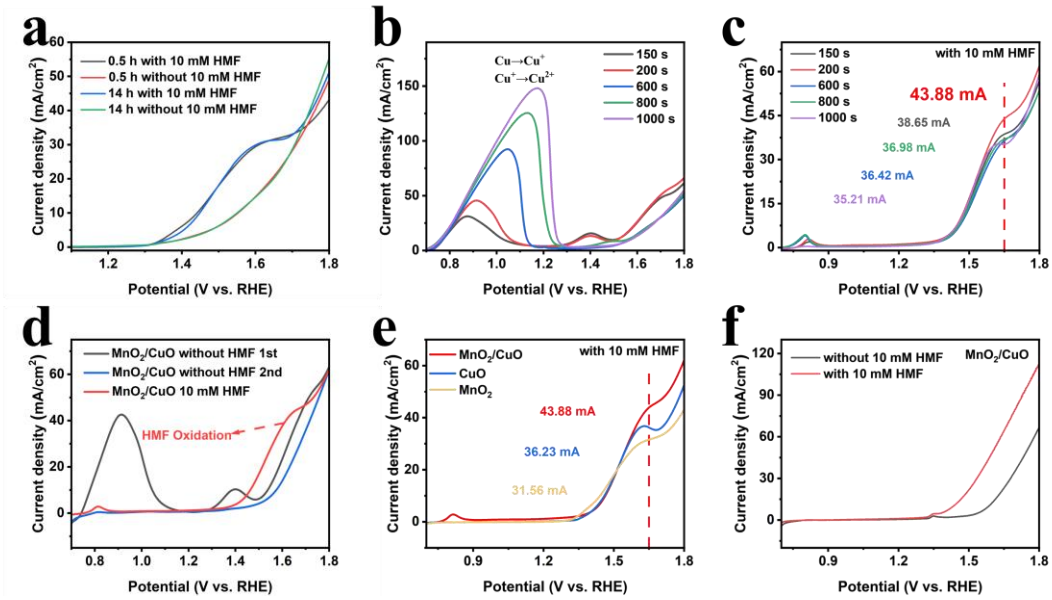

Fig. S7. (a) LSV curves of MnO_2 with different soaking times (with and without 10 mM HMF). (b) LSV curves of CuO with different electrodeposition times in 1.0 M KOH. (c) LSV curves of MnO_2/CuO with different electrodeposition times at 10 mM HMF. (d) LSV curves of MnO_2/CuO with and without 10 mM HMF. (e) LSV curves with 10 mM HMF. (f) LSV curves of MnO_2/CuO with and without 10 mM HMF (stirring conditions).

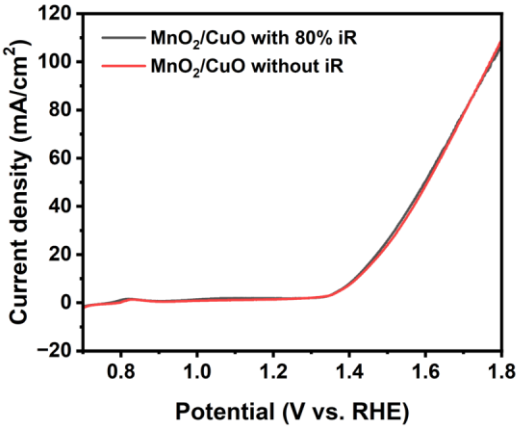

Fig. S8. LSV curves of MnO_2/CuO with and without iR (10 mM HMF).

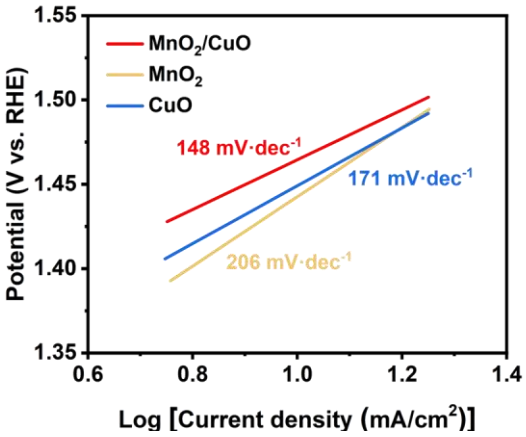

Fig. S9. Tafel slopes.

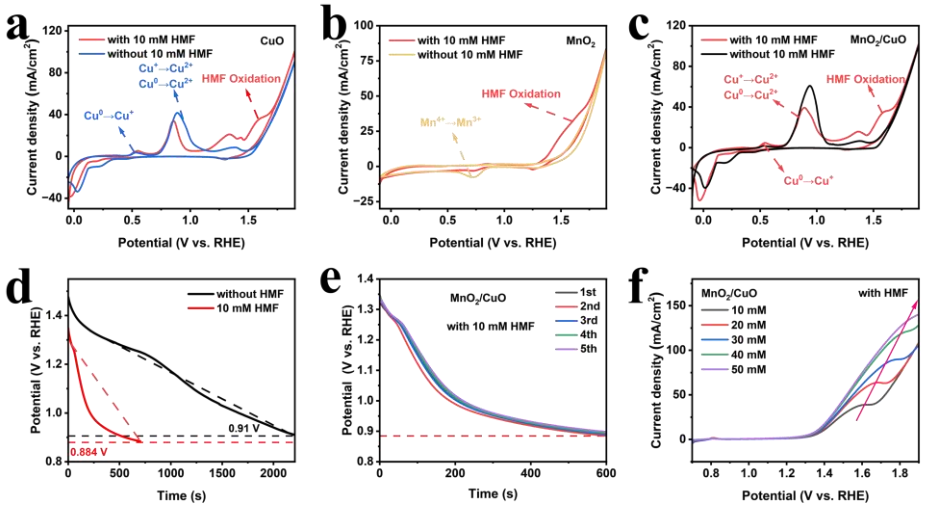

Fig. S10. CV curve of (a) CuO, (b) MnO_2, (c) MnO_2/CuO with and without 10 mM HMF. (d) Open circuit voltage vs. time. (e) Five cycles of regeneration between Cu^{2+}→Cu^{1+}. (f) LSV curves of MnO_2/CuO at different concentrations (10-50 mM HMF).

In 1.0 M KOH, the initial OCP voltage is about 1.35 V_{RHE}, which is related to the oxidation voltage of Cu^{2+}. The OCP voltage decreased to 0.91 V_{RHE} for about 2000 s. However, after the addition of 10 mM HMF, the OCP voltage quickly decreased to 0.884 V_{RHE} for only 700 s, which corresponds to the formation of Cu_2O species. The shorter decay time indirectly confirms that CuO is the main active site for HMFOR. Fig. S10e shows the regeneration experiments for five cycles of Cu^{2+}→Cu^{+}. The initial and equilibrium voltages of the five cycles are basically the same, indicating that the CuO active species underwent the spontaneous and reversible transformation on the surface of catalyst. Furthermore, the LSV experiments (10-50 mM HMF) show a linear correlation between the current density and HMF concentration (Fig. S10f), suggesting that HMFOR over MnO_2/CuO belongs to the surface-adsorption controlled process.

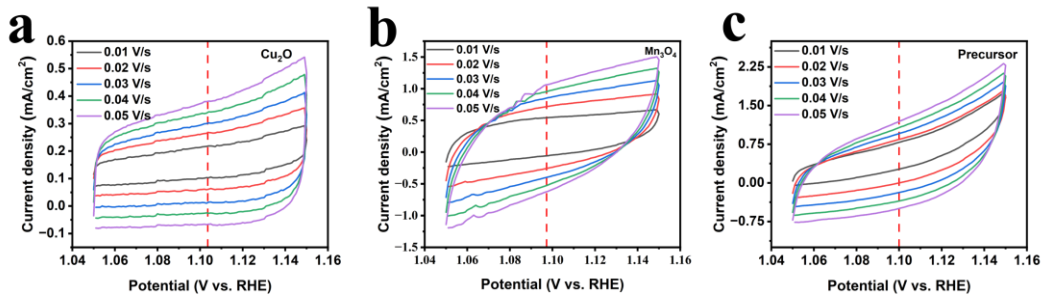

Fig. S11.CV curve of (a) Cu_2O, (b) Mn_3O_4, and (c) precursor with 10 mM HMF.

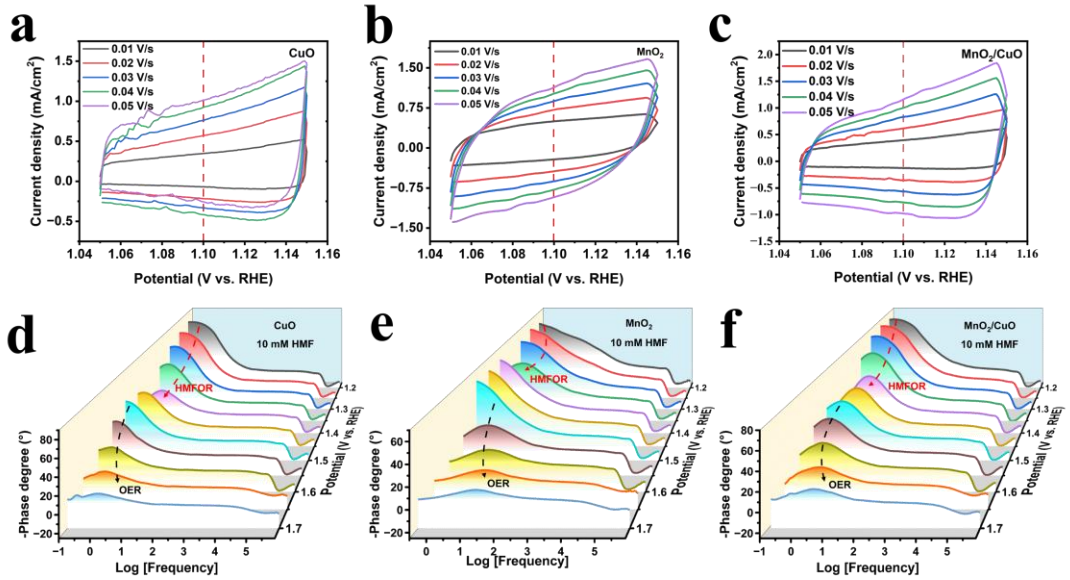

Fig. S12. CV curve of (a) CuO, (b) MnO_2, (c) MnO_2/CuO with 10 mM HMF. EIS spectra of (d) CuO, (e) MnO_2, (f) MnO_2/CuO with 10 mM HMF.

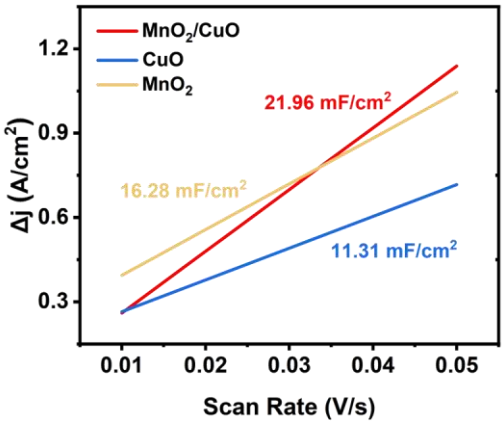

Fig. S13. Cdl of CuO, MnO_2 and MnO_2/CuO.

The inherent electrocatalytic performances are estimated by the electrochemically surface area (ECSA) of CuO, MnO_2 and MnO_2/CuO (Fig. S11, Fig. S12a-c). The double-layer capacitance (Cdl) has a linear relationship with ECSA, which could be measured by CV curves at different scan rates. As shown in Fig. S13, the Cdl in 10 mM HMF is 11.31, 16.28 and 21.96 $mF \cdot cm^{-2}$ for CuO, MnO_2 and MnO_2/CuO, respectively. The larger ECSA of MnO2/CuO indicates that MnO_2/CuO have better electrocatalytic ablilty than the bare CuO and MnO_2.

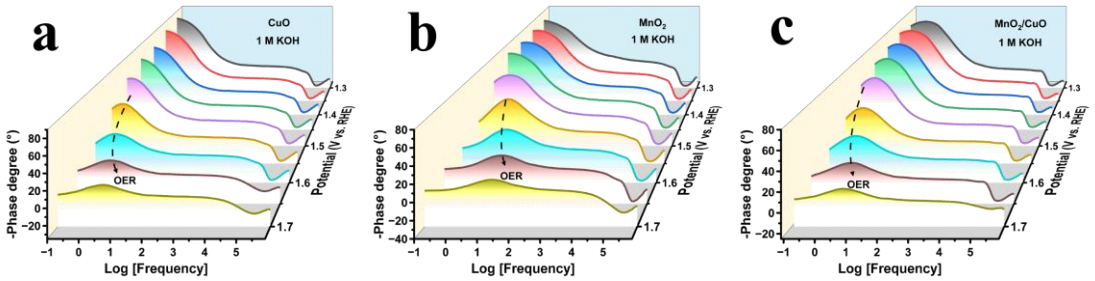

Fig. S14. EIS spectrum of (a) CuO, (b) MnO_2, and (c) MnO_2/CuO with 1.0 M KOH.

The difference in reaction kinetics between OER and HMFOR is further investigated by the electrochemical impedance spectroscopy (EIS) to account for the interfacial electrochemical behavior during HMFOR. EIS tests are performed on CuO, MnO_2 and MnO_2/CuO in 1.0 M KOH and 10 mM HMF solutions, respectively. As shown in Fig. S14a-c, OER begin to appear in the low frequency region (0.1-10 Hz) since 1.5 V_{RHE}, which reveals the slow kinetics of water oxidation. In the intermediate frequency region (10-102 Hz), a new peak responding to HMFOR appeared from 1.35 V_{RHE}, which is also consistent with LSV results.

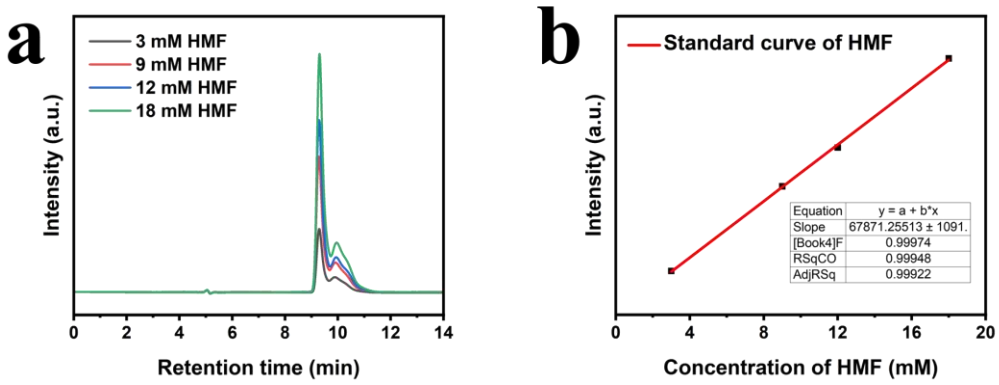

Fig. S15. (a) HPLC measurements of pure HMF. (b) Calibration of HPLC for HMF.

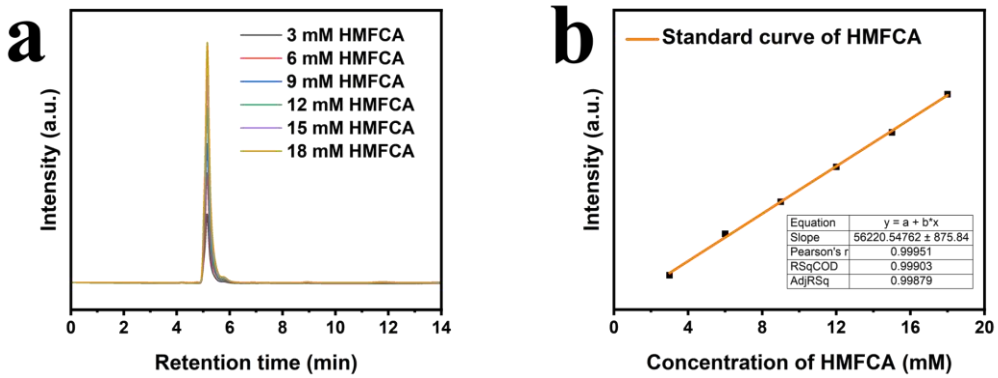

Fig. S16. (a) HPLC measurements of pure HMFCA. (b) Calibration of HPLC for HMFCA.

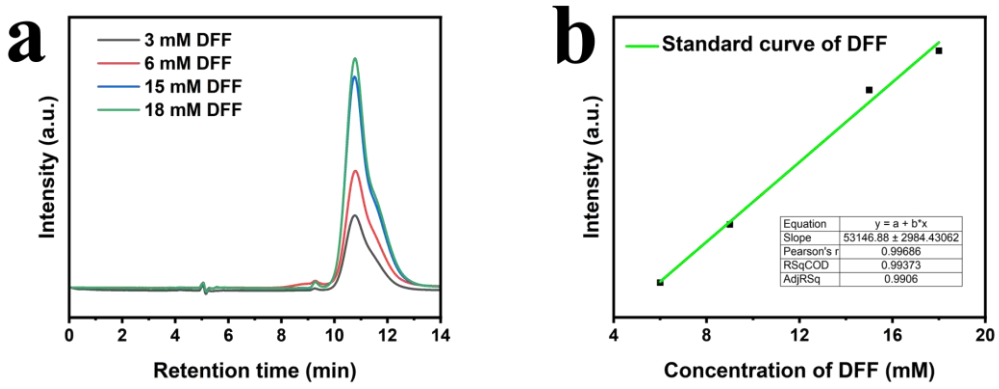

Fig. S17. (a) HPLC measurements of pure DFF. (b) Calibration of HPLC for DFF.

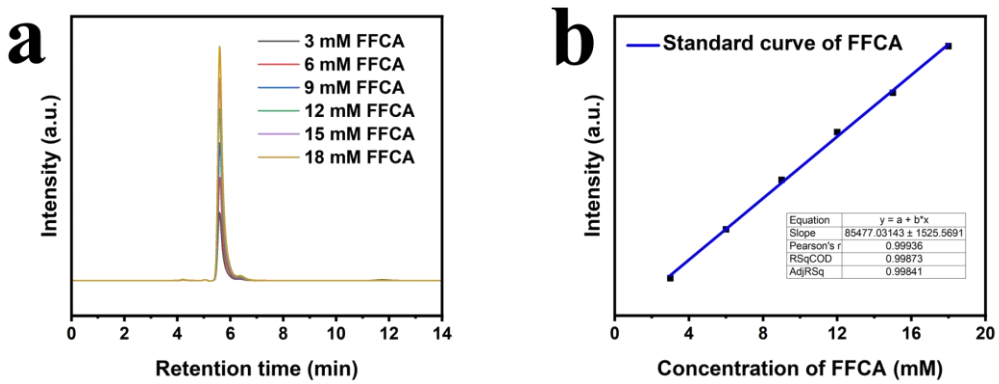

Fig. S18. (a) HPLC measurements of pure FFCA. (b) Calibration of HPLC for FFCA.

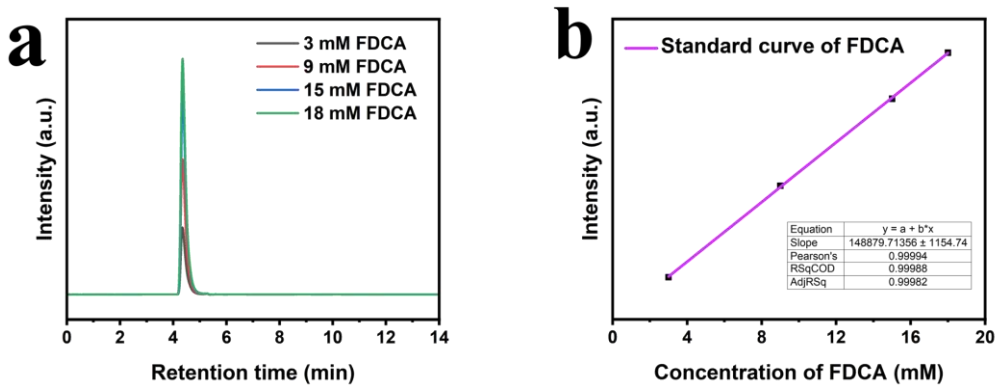

Fig. S19. (a) HPLC measurements of pure FDCA. (b) Calibration of HPLC for FDCA.

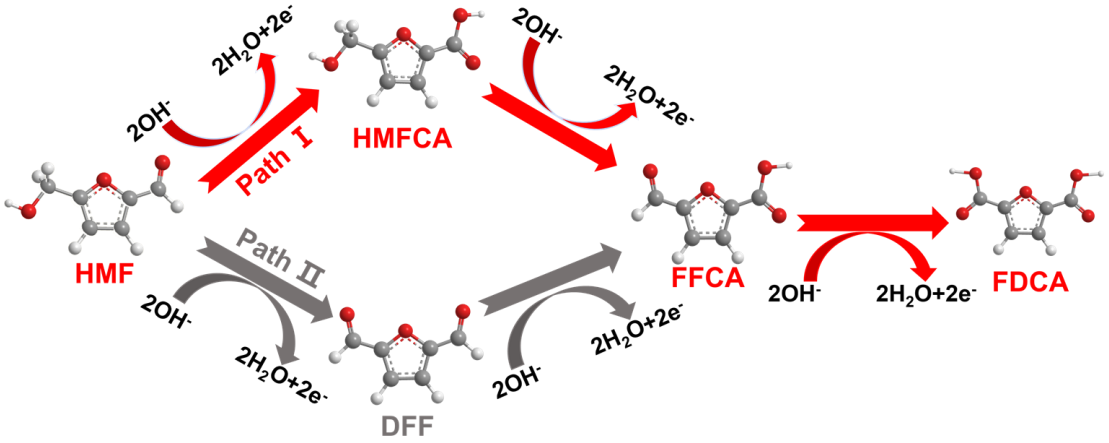

Fig. S20. Two alternative pathways for HMFOR.

The following reactions are performed at the anode and cathode of the cell:

Anodic reaction: $HMF(l) + 6OH^-(aq) \rightarrow FDCA(l) + 4H_2O(l) + 6e^-$

Cathodic reaction: $6H_2O(l) + 6e^- \rightarrow 3H_2(g) + 6OH^-(aq)$

Total response: $HMF(l) + 2H_2O(l) \rightarrow FDCA(l) + 3H_2(g)$

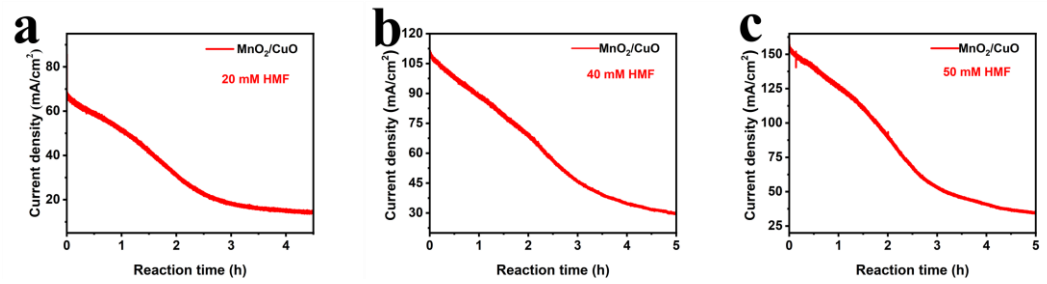

Fig. S21. The curve of current density vs time over the MnO_2/CuO (1.0 M KOH) (a) 20 mM HMF. (b) 40 mM HMF. (c) 50 mM HMF.

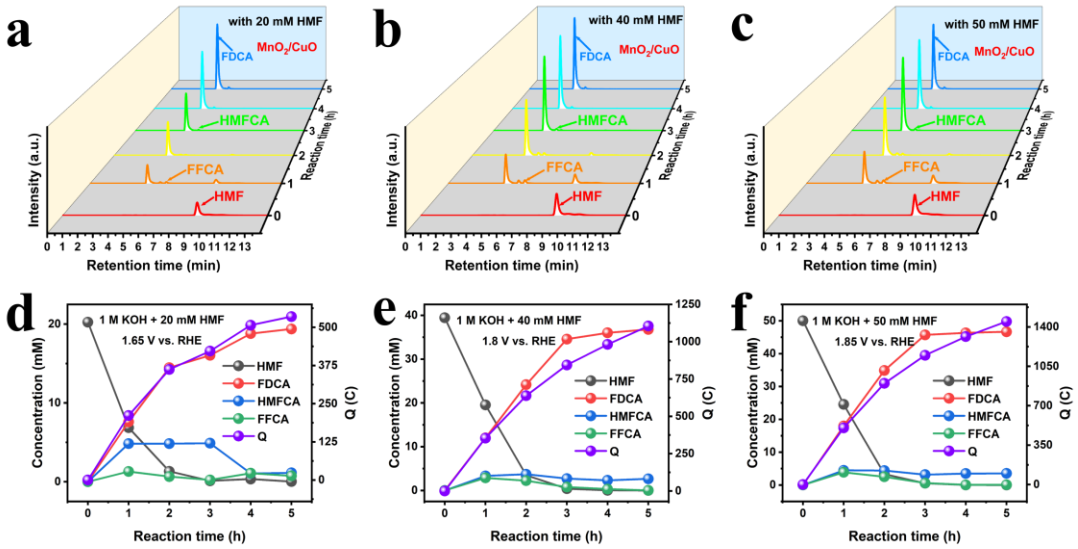

Fig. S22. HPLC chromatogram of MnO_2/CuO at (a) 20 mM, (b) 40 mM and (c) 50 mM HMF concentrations. Concentration of HMF, FDCA, HMFCA, FFCA and total charge vs time over the MnO_2/CuO (d) 20 mM, (e) 40 mM and (f) 50 mM HMF concentrations.

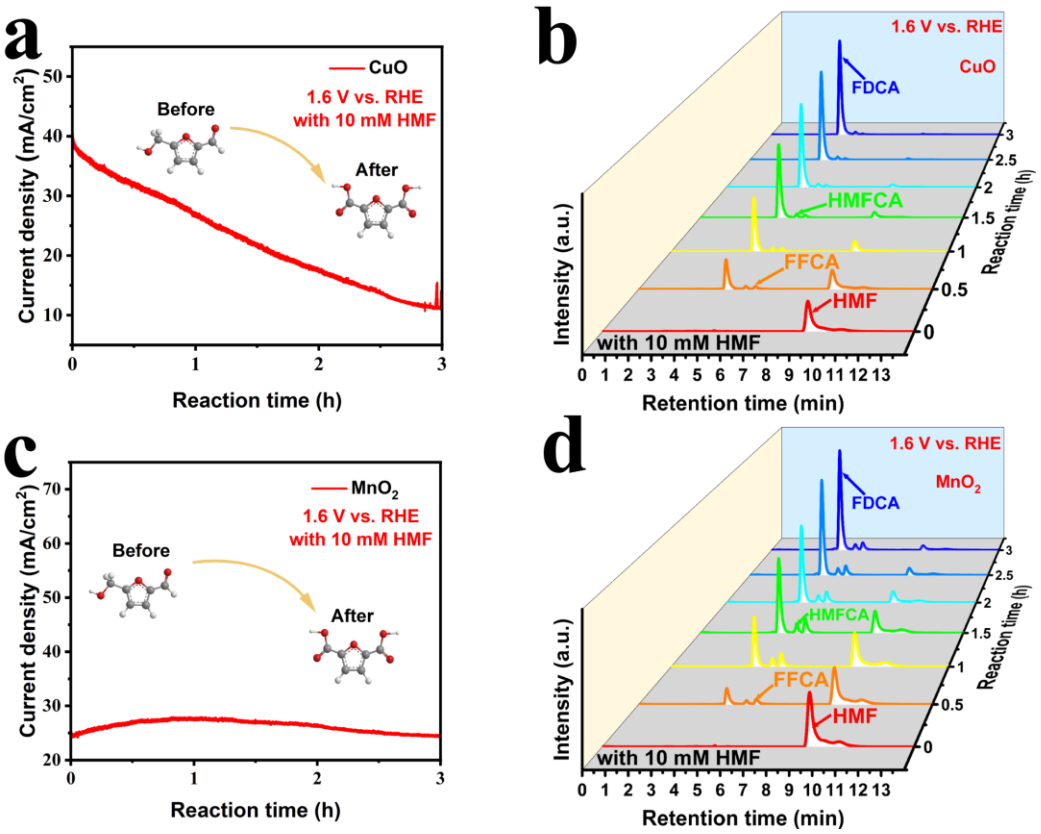

Fig. S23. The curve of current density vs time over (a) CuO, and (c) MnO_2. HPLC chromatogram of the (b) CuO, and (d) MnO_2.

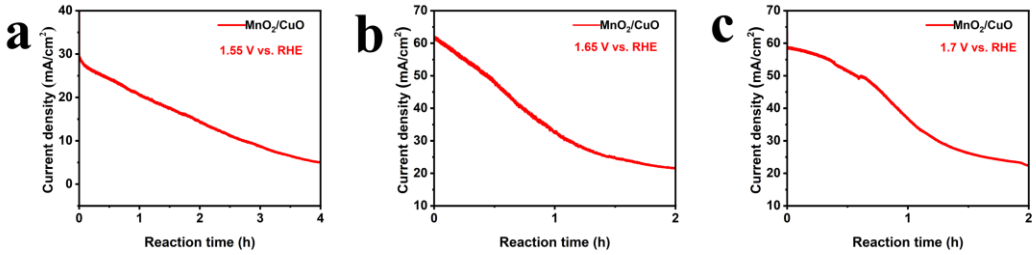

Fig. S24. The curve of current density vs time over the MnO_2/CuO at (a) 1.55 V_{RHE}, (b) 1.65 V_{RHE}, and (c) 1.7 V_{RHE} (10 mM HMF, 1 M KOH). HPLC chromatogram of the MnO_2/CuO at (d) 1.55 V_{RHE}, (e) 1.65 V_{RHE}, and (f) 1.7 V_{RHE} (10 mM HMF, 1.0 M KOH).

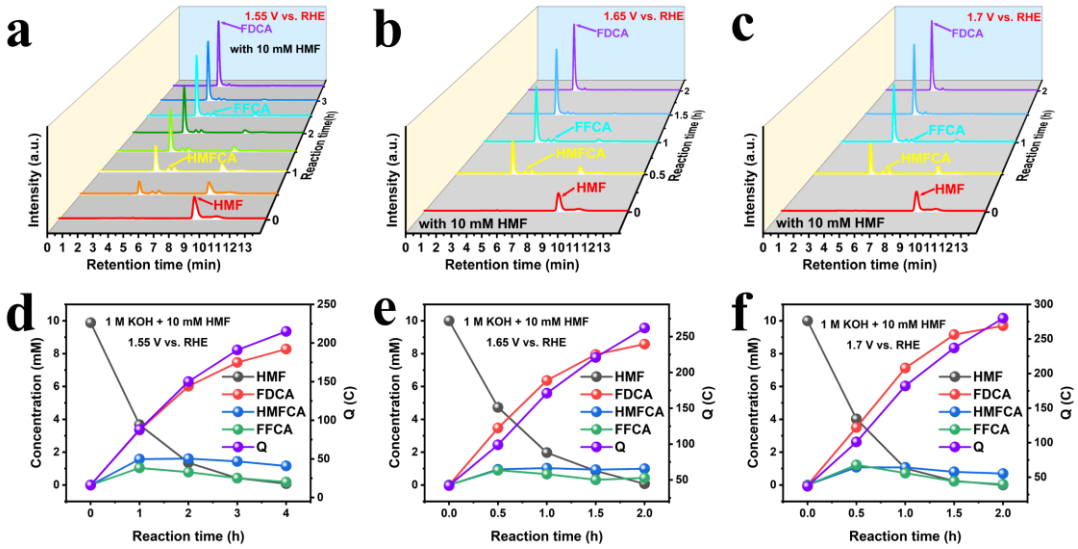

Fig. S25. HPLC chromatogram of the MnO_2/CuO at (a) 1.55 V_{RHE}, (b) 1.65 V_{RHE}, and (c) 1.7 V_{RHE} (10 mM HMF, 1.0 M KOH). Concentration of HMF, FDCA, HMFCA, FFCA and total charge vs time over the MnO_2/CuO at (d) 1.55 V_{RHE}, (e) 1.65 V_{RHE} , and (f) 1.7 V_{RHE} (10 mM HMF, 1.0 M KOH).

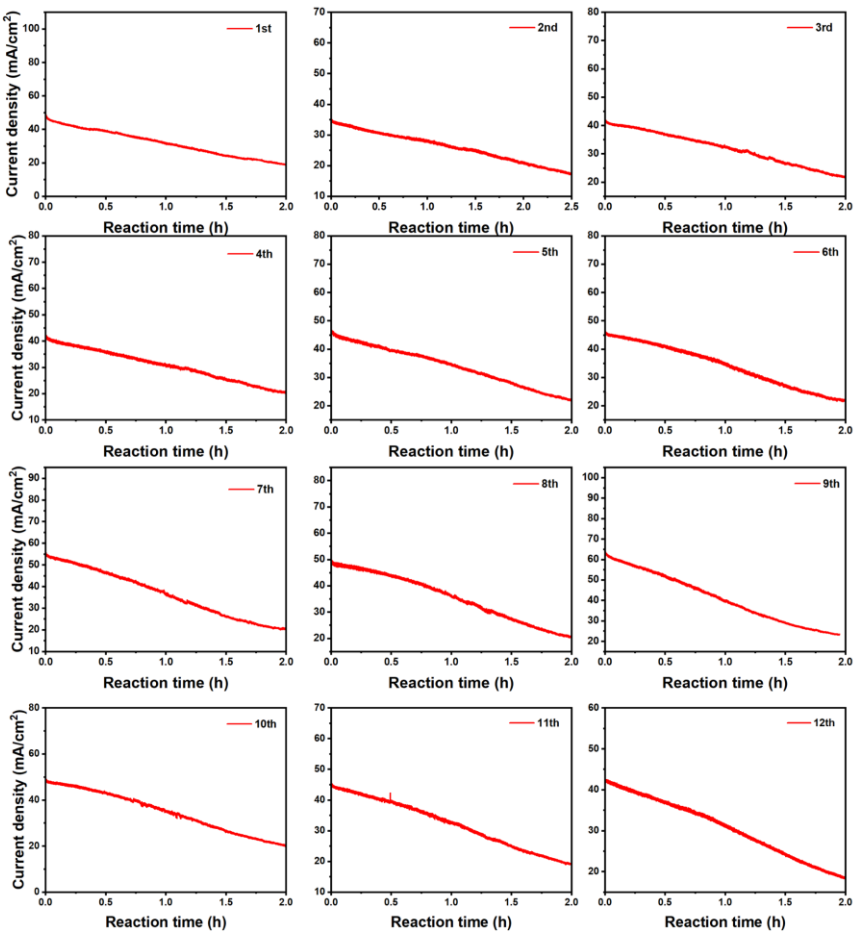

Fig. S26. The curve of current density vs time over the MnO_2/CuO (1.0 M KOH, twelve consecutive cycles)

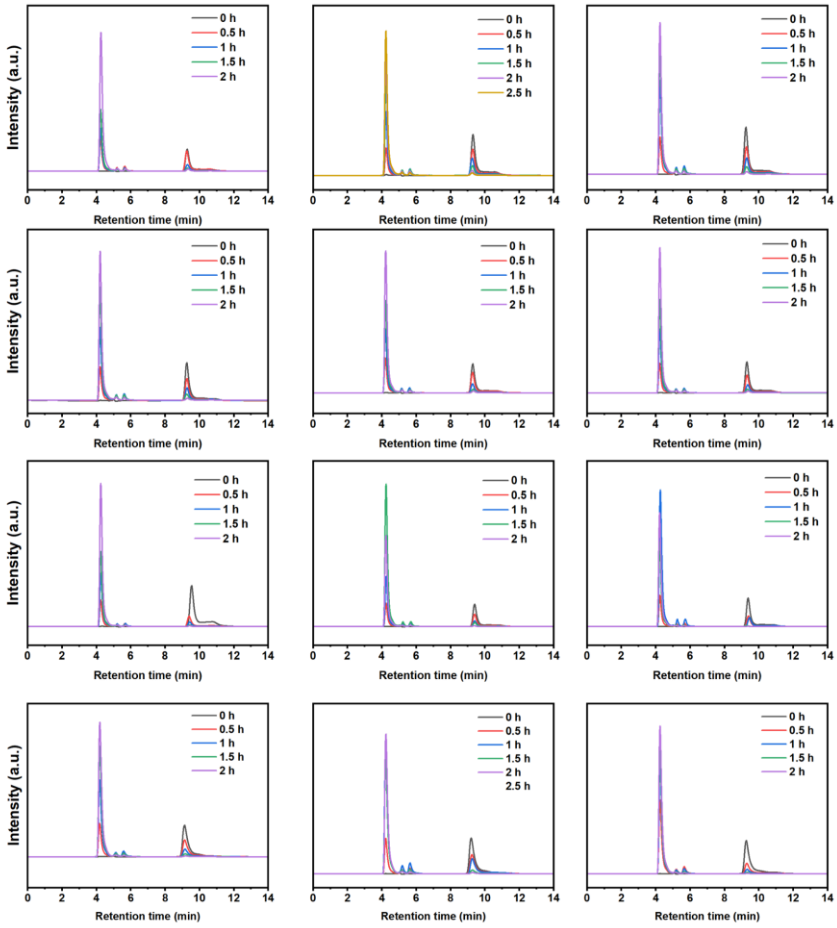

Fig. S27. HPLC chromatogram of twelve consecutive cycles of MnO_2/CuO.

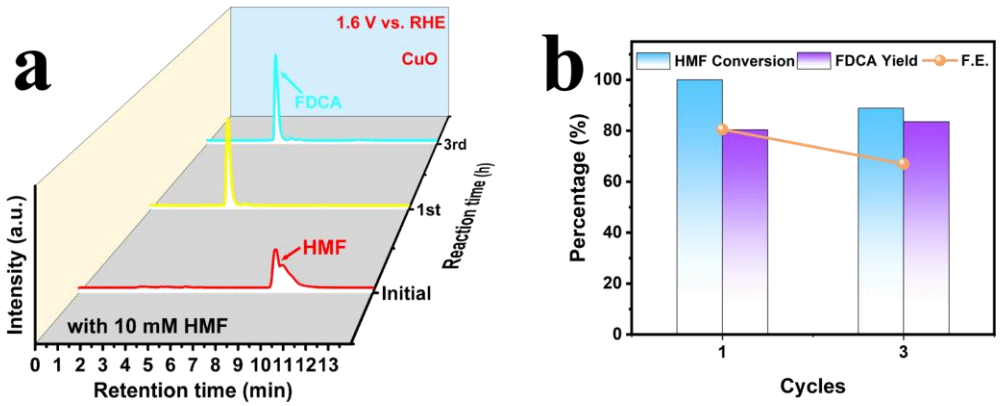

Fig. S28. (a) HPLC chromatogram of the CuO (three cycles). (b) HMF conversion, FDCA yield and FE over CuO during three successive of HMF oxidations (1.6 V_{RHE}, 10 mM HMF, 1.0 M KOH).

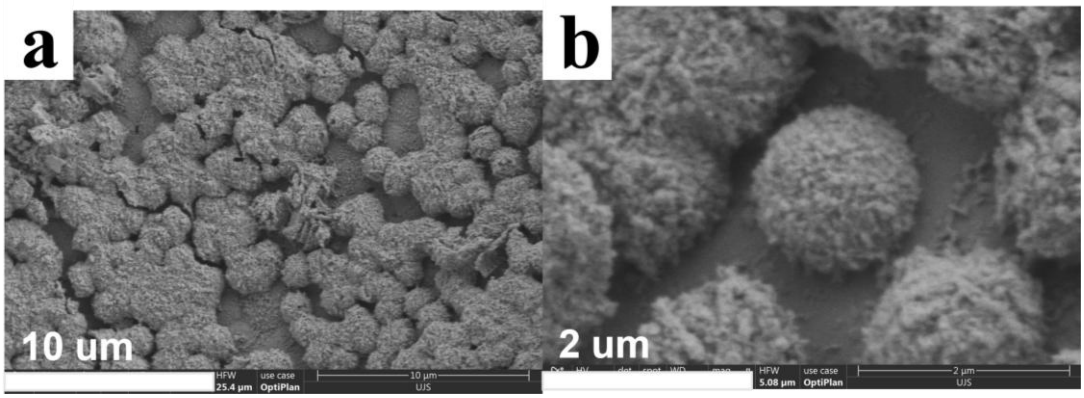

Fig. S29. SEM images of MnO_2/CuO after twelve consecutive cycles(low magnification).

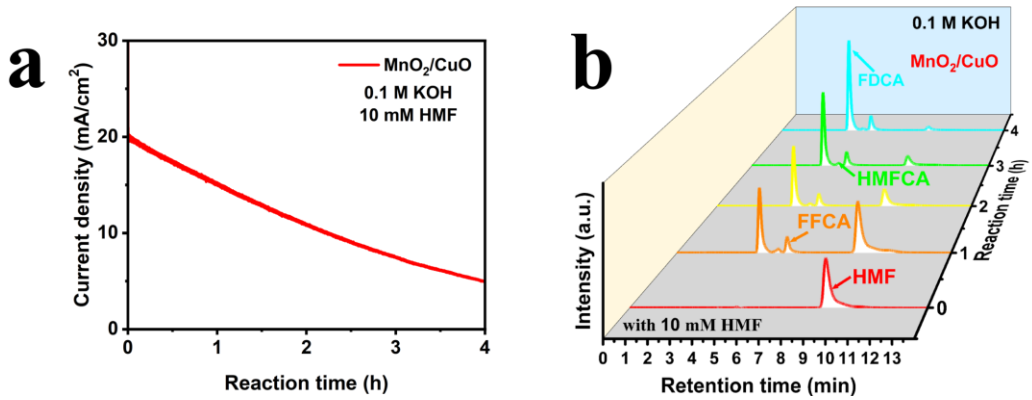

Fig. S30. (a) The curve of current density vs time over the MnO_2/CuO (10 mM HMF, 0.1 M KOH). (b) HPLC chromatogram of the MnO_2/CuO (10 mM HMF, 0.1 M KOH).

The effect of low OH^- concentration (0.1 M KOH) on the selectivity during HMFOR is also investigated. Compared with 1 M KOH, the HMF conversion and FDCA yield of the reaction decreased. Interestingly, DFF is not found in the intermediate during the reaction. Therefore, it further confirms that reaction pathway I takes the dominant position. The concentration of intermediate FFCA is noticeably higher than that of HMFCA in 0.1 M KOH. However, in 1 M KOH, the concentration of HMFCA is distinctly higher than that of FFCA. The concentration of the intermediate FFCA is significantly higher than that of HMFCA in 0.1 M KOH, which is different from the results in 1.0 M KOH. Therefore, it is speculated that the oxidation of FFCA to FDCA is the rate-determining step (RDS) of HMFOR in 0.1 M KOH. Whereas, in 1.0 M KOH solution, the conversion of HMFCA to FFCA is the RDS of the HMFOR reaction.

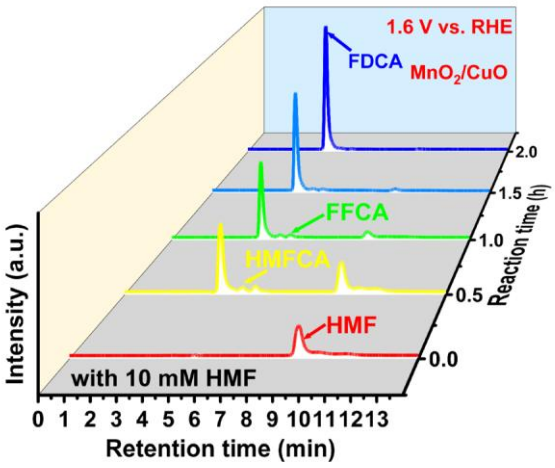

Fig. S31. HPLC chromatogram of the MnO_2/CuO in flow electrolytic cell (10 mM HMF, 1.0 M KOH).

Compared with H-type electrolytic cell, the continuous flow electrolytic cell can realize the continuous supply of reactants and product of FDCA, which effectively prevents the polarization of solution concentration and improves the mass transfer efficiency of substances. The MnO_2/CuO with an area of 1 cm2 are prepared and mounted on the anode of the continuous flow electrolytic cell, and proton exchange membrane is installed between the anode and the cathode. Experiments in a continuous flow electrolytic cell can better simulate the actual industrial production and provide strong evidence for the practical application value of the catalyst.

Table S1. Comparison of HMFOR performance for MnO_2/CuO and other reported catalysts

Entry	Catalyst	Potential (V vs.RHE)	HMF concentration (mM)	Electrolyte	FDCA Yield (%)	FE (%)	Ref
1	Cu NPS with Fe^{3+}	1.57	10	1.0 M KOH	70.3	70.3	[1]
2	Co_1Cu_1-CH	1.57	10	1.0 M KOH	90.0	70.0	[2]
3	$Ni_xCo_{3-x}O_4$	1.60	10	1.0 M KOH	-	78.0	[3]
4	CuO/Co_3O_4	1.60	10	1.0 M KOH	-	79.8	[4]
5	$N\text{-}MoO_2/Ni_3S_2$	1.57	10	1.0 M KOH	90.0	90.0	[5]
6	Ni MOF/Ag	1.623	10	1.0 M KOH	98.6-	98.6-	[6]
7	$NF@Co_3O_4/CeO_2$	1.60	10	1.0 M KOH	30.2	55.2	[7]
8	Co_3O_4-NiO-500	1.45	10	0.1 M KOH	83.33	89.47	[8]
9	CuO-PdO	-	50	1.0 M KOH	96.2	93.7	[9]
10	CF−CuO/CeO_2	1.61	10	1.0 M KOH	99.7	97.9	[10]
11	Cu_2P_7-CoP (1 : 5)	1.43	10	1.0 M KOH	98.8	98	[11]
12	14%Ce-$Ni(OH)_2$	1.56	10	1.0 M KOH	97.8	86.6	[12]
13	P-Co_3O_4-NBA@NF	1.636	10	1.0 M NaOH	96.9	97.0	[13]
14	NiS_x/Ni_2P	1.46	10	1.0 M KOH	98.5	95.1	[14]
15	NiO/CeO_2@NF	1.575	10	1.0 M KOH	90.0	83.0	[15]
16	MnO_2/CuO	1.60	10	1.0 M KOH	98.0	98.2	**This work**

References

(1) Zhou, Y.; Shen, Y.; Li, H. Mechanistic study on electro-oxidation of 5-hydroxymethylfurfural and water molecules via operando surface-enhanced Raman

spectroscopy coupled with an Fe3+ probe. *Applied Catalysis B: Environmental* **2022**, *317*, 121776.

(2) Li, H.; Huang, X.; Lv, Y.; Zhang, J.; Li, W. Highly efficient electrooxidation of 5-hydroxymethylfurfural (HMF) by Cu regulated Co carbonate hydroxides boosting hydrogen evolution reaction. *International Journal of Hydrogen Energy* **2023**, *48* (97), 38279-38295.

(3) Zhou, Z.; Xie, Y.-n.; Sun, L.; Wang, Z.; Wang, W.; Jiang, L.; Tao, X.; Li, L.; Li, X.-H.; Zhao, G. Strain-induced in situ formation of NiOOH species on CoCo bond for selective electrooxidation of 5-hydroxymethylfurfural and efficient hydrogen production. *Applied Catalysis B: Environmental* **2022**, *305*, 121072.

(4) Zhang, L.; Jin, P.; Wu, Z.; Zhou, B.; Jiang, J.; Deng, A.; Li, Q.; Hussain, T.; Zhang, Y.; Liu, H. CuO/Co3O4 Bifunctional Catalysts for Electrocatalytic 5-Hydroxymethylfurfural Oxidation Coupled Cathodic Ammonia Production. *Energy & Environmental Materials* **2024**, e12725.

(5) Wang, L.; Cao, J.; Lei, C.; Dai, Q.; Yang, B.; Li, Z.; Zhang, X.; Yuan, C.; Lei, L.; Hou, Y. Strongly coupled 3D N-doped MoO2/Ni3S2 hybrid for high current density hydrogen evolution electrocatalysis and biomass upgrading. *ACS Applied Materials & Interfaces* **2019**, *11* (31), 27743-27750.

(6) Pang, X.; Zhao, H.; Huang, Y.; Luo, B.; Bai, H.; Fan, W. Electrochemically induced NiOOH/Ag+ active species for efficient oxidation of 5-hydroxymethylfurfural. *Applied Surface Science* **2023**, *608*, 155152.

(7) Zhao, G.; Hai, G.; Zhou, P.; Liu, Z.; Zhang, Y.; Peng, B.; Xia, W.; Huang, X.; Wang, G. Electrochemical oxidation of 5-hydroxymethylfurfural on CeO2-modified Co3O4 with regulated intermediate adsorption and promoted charge transfer. *Advanced Functional Materials* **2023**, *33* (14), 2213170.

(8) Jin, P.; Zhang, L.; Wu, Z.; Zhou, B.; Duan, Z.; Li, H.; Liu, H.; Deng, A.; Li, Q.; Zhang, Y. Heterogeneous interface induced Co3O4-NiO catalyst for efficient electrocatalytic 5-Hydroxymethylfurfural oxidation. *Chemical Engineering Journal* **2024**, *481*, 148303.

(9) Zhou, P.; Lv, X.; Tao, S.; Wu, J.; Wang, H.; Wei, X.; Wang, T.; Zhou, B.; Lu, Y.; Frauenheim, T. Heterogeneous-interface-enhanced adsorption of organic and hydroxyl for biomass electrooxidation. *Advanced Materials* **2022**, *34* (42), 2204089.

(10) Pang, X.; Zhao, H.; Huang, Y.; Liu, Y.; Bai, H.; Fan, W.; Shi, W. In situ electrochemical reconstitution of CF–CuO/CeO2 for efficient active species generation. *Inorganic Chemistry* **2022**, *61* (23), 8940-8954.

(11) Bi, J.; Xu, H.; Wang, W.; Sang, T.; Jiang, A.; Hao, J.; Li, Z. Cu2P7-CoP Heterostructure Nanosheets Enable High-Performance of 5-Hydroxymethylfurfural Electrooxidation. *Chemistry–A European Journal* **2023**, *29* (42), e202300973.

(12) Huang, Y.; Pang, X.; Cui, J.; Huang, Z.; Wang, G.; Zhao, H.; Bai, H.; Fan, W. Strengthening the stability of the reconstructed NiOOH phase for 5-hydroxymethylfurfural oxidation. *Inorganic Chemistry* **2023**, *62* (16), 6499-6509.

(13) Liu, D.; Li, Y.; Wang, C.; Yang, H.; Wang, R.; Li, S.; Yang, X. Numerous active sites in self-supporting Co3O4 nanobelt array for boosted and stabilized 5-hydroxymethylfurfural electro-oxidation. *Applied Catalysis A: General* **2024**, *669*, 119497.

(14) Zhang, B.; Fu, H.; Mu, T. Hierarchical NiS x/Ni 2 P nanotube arrays with abundant interfaces for efficient electrocatalytic oxidation of 5-hydroxymethylfurfural. *Green Chemistry* **2022**, *24* (2), 877-884.

(15) He, X.; Mo, Z.; Liu, H.; Wang, C. Interface engineering of the NiO/CeO 2@ NF heterostructure to boost the electro-oxidation of 5-hydroxymethylfurfural. *Dalton Transactions* **2023**, *52* (27), 9456-9464.